Workshop on Visualisation in Environmental Sciences (EnvirVis) (2017)
R. Bujack and A. Middel and K. Rink and D. Zeckzer (Editors)

Visual Study of the Benguela Upwelling System using Pathline Predicates

P. Nardini[1] , M. Böttinger[2] , G. Scheuermann[1] , M. Schmidt[3]

[1]Image and Signal Processing Group, University of Leipzig, Germany
[2]German Climate Computing Center (DKRZ), Hamburg, Germany
[3]Leibniz Institute for Baltic Sea Research (IOW), Warnemünde, Germany

Abstract

Due to the nutrient-rich water transported to the upper layer of the ocean, coastal upwelling systems are regions especially important for marine life and fishery. In this work, we focus on a visual analysis of the spatio-temporal structure of the Benguela upwelling system using pathline predicates. Based on the 3D flow field from an ocean model simulation, we first derive space-filling trajectories covering the full model grid. From these, we select and visualize pathlines related to upwelling. In a second step, we derive a 3D scalar field representing the pathline density, which is visualized using volume rendering techniques. Further analyses of the pathlines show a distinct annual cycle in the upwelling activity, which fits well to observation-based analyses found in literature.

Categories and Subject Descriptors (according to ACM CCS): I.3.3 [Computer Graphics]: Picture/Image Generation—Line and curve generation Computer Applications [J.2]: Earth and atmospheric sciences—

1. Introduction

Coastal upwelling systems are regions characterized by relatively cool nutrient-rich water, which "disproportionally contribute to the global primary production and host many of the major commercially used fish stocks" [MEJ*14]. Due to their importance to marine life and fishery, coastal upwelling regions such as the Benguela, located off the coast of Namibia and South Africa, are in focus of ongoing scientific observation campaigns and modeling activities. Coastal upwelling is a dynamical process driven by wind stress at the sea surface, which is characterized by the transport of cool water from greater to shallower depths. Consequently, areas affected can be identified by pronounced negative anomalies in the sea surface temperature (STT). Hagen et al. [HFAO01] concluded that "intense upwelling generates SST of less or equal to 13°C". However, although the surface of water masses transported by upwelling can e.g. be located through SST anomalies, the spatial upwelling process cannot directly be visualized simply by displaying single variables. Furthermore, the Benguela upwelling shows a distinct seasonal and interannual variability [HFAO01, TZH15], which requires studying longer time periods for further analyses.

In this work we focus on the visual analysis of the coastal upwelling process on the basis of time-dependent flow fields using the Benguela system as an example. More specifically, we apply proven methods such as particle tracing in order to identify the structure of the flow contributing to upwelling. Trajectories illustrate the connectivity between different ocean areas and different depth levels. Finally, we derive upwelling-related scalar fields by filtering and further analyzing relevant trajectories, which then allow applying scalar field visualization techniques to study the spatio-temporal structure at interactive frame rates. In the remainder of this article, we discuss related work and give a brief overview on the simulation data we used, before we explain the methodology used for selecting and visualizing only those parts of the flow field relevant to upwelling.

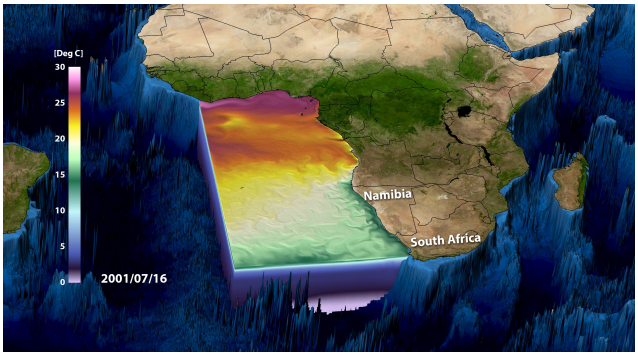

Figure 1: *The visualization of water temperature shows the 3D model domain. Note the cool water (dark green color) along the coast off Namibia and South Africa, which characterizes the Benguela upwelling system at the sea surface.*

DOI: 10.2312/envirvis.20171099

2. Related Work

Although coastal upwelling is a research area of high societal and environmental relevance, only little work has been published specifically with respect to visualizing the upwelling process. In ocean sciences, mainly 2D methods have been used in recent publications (cf. [MEJ*14, MRS*14, TZH15]): 2D-slices of either simulation data or observations are visualized to display snapshots of the phenomenon, and temporal evolutions are analyzed with XY-plots of integral quantities or Hovmoeller-type 2D-diagrams [Hov49]. Su and Sheng [SS99] visualized the upwelling process in the Monterey Bay area by employing a GIS system to prepare and filter the data and by using the interactive 3D visualization system Vis5D [HS90] for the actual visualization. Isosurfaces were used to display the spatial structure of temperature, salinity and density.

Beyond these activities, a variety of methods for time-dependent flow field visualization has been developed by the visualization community and applied to different use cases. The survey of McLoughlin et al. [MLP*09] summarizes the state-of-the-art in *geometric flow visualization*, where the flow field is visualized by tracing pathlines (trajectories) of objects placed in the flow. Laramee et al. [LHD*04] surveyed *texture-based methods*, which create dense representations of the flow. Overviews of *feature- and topology-based* methods are given in [PVH*03] and [LHZP07, HLH*16]. A survey of *partition-based flow* visualization can be found in [SWJS08]. Recent related work include [CLSW14], who defined a *streamline box counting ratio* to derive the space-filling capacity of streamlines in order to use that as a predicate for filtering of streamline segments. Sprenger and Wernli developed the analysis tool for Lagrangian flow LAGRANTO [SW15], which provides flexible means to first seed trajectories and then make selections based on geometrical or meteorological criteria. Kanzler et al. presented an approach to "adaptively control the line density of streamlines and trajectories based on the importance of lines and their occlusions" [KFW16]. The idea of using streamline and pathline predicates was introduced by Salzbrunn [SS06, SGSM08]. Using MRI data, Born et al. applied pathline predicates to select trajectories optimally suited for visualizing blood flow [BPMS12, BMGS13].

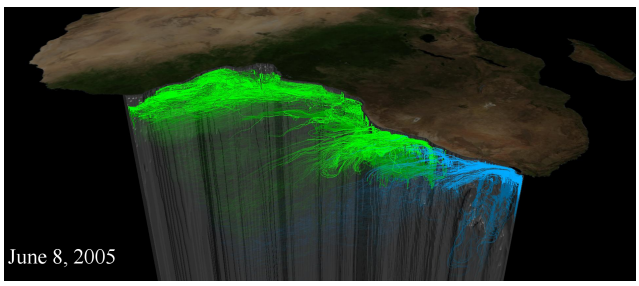

Figure 2: *Line-based visualization of the trajectories for particles encountering upwelling on June 4, 2005. Trajectories entering the domain at the western boundary are shown in green, those starting at the southern border are shaded blue. Transparency mapping was additionally used to encode the distance to the upwelling region. The visualization has a scale-factor in z-direction (depth) of 4000.*

3. Simulation Data

For this work, we used the ocean flow field and a synthetic tracer field from numerical simulations carried out with a regional coupled ocean biogeochemistry model. The numerical simulations and the ocean model MOM version 4 used for the hydrodynamical part therein are described in [GGD*05, HSGL11, SE16]. The model domain covers the southeast Atlantic, as shown in Figure 1, and is represented by a rectilinear grid of the size 268 x 377 x 89. "Dry" grid cells (land) are masked out with a special value to prevent them from being used in the analysis. The data used consists of 5-day-means for a time period of approximately 12 years. The NetCDF file containing the whole time series of the three velocity components *(u,v,w)* has a size of about 100 GB.

4. Methods

Since pathlines potentially capture the complete history of particles in spatio-temporal flow fields, we decided to use a geometric flow visualization method to analyze the upwelling.The problem of seeding has been widely discussed in literature and is still an active research area: Where in space and time do particles need to be seeded for capturing the process being studied? We selected the methodology developed by Salzbrunn et al. and Born et al. [SS06, SGSM08, BPMS12, BMGS13], *pathline predicates*, to first compute particle pathlines filling the entire 3D model grid and then select and visualize those we are interested in. In order to achieve a Langrangian representation of the vector field, we seeded one weightless particle into each cell of the computational grid.We chose to use the Euler method for the pathline integration. For every further time step, we seeded new particles in all empty cells. The large amount of pathlines computed was filtered with respect to problem-specific user-defined predicates. We proposed "upwelling predicates" by defining a minimal starting depth, a minimum depth, and a minimal angle of ascent, which were then used for filtering trajectories.

With respect to the interactive performance of line-based trajectory visualizations, we further reduced the information by deriving the *local pathline density* **LPD**, a scalar measure for the accumulated length of all trajectory line segments traversing a cell. We derived the LPD for each time step. Additionally, we derived a second scalar representing particles contributing to upwelling. For this, we derived the number of particles present in a cell for each time step. Since the trajectory of each particle is known, we can differentiate between particles encountering upwelling during their lifetime and particles not related to upwelling. The ratio between upwelling particles and other particles in each cell, which we call *upwelling particle ratio* **UPR**, is then visualized using a volume rendering technique. To obtain a dense representation of the vector field by the use of trajectories, we ensure that each ocean cell at least contains one particle throughout all time steps. For each of the seeding points, the full simulation time span is taken into account by forward and backward integration of the trajectories. To save computing time, we used the relatively simple but fast Euler method for the trajectory integration. Our algorithm seeds a particle into the center of every ocean cell and integrates the pathlines step by step. At each time step, all cells are checked for the presence of at least one particle; new particles are inserted if cells are found

empty. The advection algorithm has been modified to account for the no-flux boundary conditions at the sea floor. Furthermore trajectories must not intersect the sea surface but are allowed to leave the ocean domain at the western or southern open boundary. This is achieved with an adaptive choice of the time step size. We used a start/maximum step size of 10 hours and a minimum step size of 15 minutes. With these settings, the methodology yielded 123 million trajectories, which is a spatially dense representation of the flow described by the 3D vector field for the entire simulation period. However, the full trajectory set had to be tested for upwelling predicates.

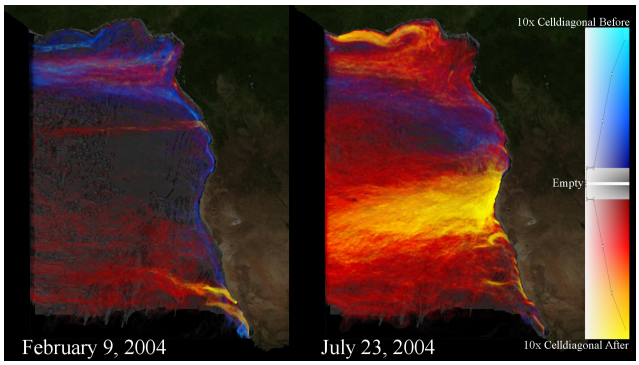

Figure 3: *Top view of volume renderings of LPD for two seasons. LPD before upwelling is shaded in blue, after upwelling the colors range from red to yellow. The line in the colorbar denotes the opacity value (left = no opacity, right = full opacity).* ***Left****: Low LPD in austral summer;* ***Right****: High LPD in austral winter.*

4.1. Upwelling Trajectories

In this subsection, we describe the trajectory filtering. First we define three different pathline predicates that characterize upwelling flow. In the Benguela upwelling system, the source water mass of upwelling usually stems from 100 to 200m depth [JSM15].Therefore, we first define a minimum depth particles must have had before they are welled up. Second, we need to find a predicate for the ascent of water towards the surface. To check this condition, we calculate the angle to the z-axis for each segment of a trajectory. If this angle exceeds a defined threshold, the second requirement is fulfilled. Lastly, it must be ensured that the rising water reaches the upper water levels or even the sea surface. Therefore, we define a second (shallower) depth level that must be passed. We define *upwelling-time* (**uw-time**) as the time at which a trajectory first fulfills all requirements. This time is then used to temporally cluster trajectories representing upwelling within the same time frame. For our analysis, we used 50m for both depth requirements, and the trajectories had to ascend with a minimum angle of 60°. With these settings, we identified 7 million upwelling trajectories for the complete simulation.

Line-based visualizations of all pathlines with the same uw-time were found to be quite overcrowded and did not reveal much insight. To further improve the visualization, we evaluated and visualized the entry points of the trajectories into the domain by using different colors. We identified two major currents entering the domain. The Equatorial Undercurrent and the South Equatorial Counter Current enter the model domain from the west, bending poleward at the African coast. From the south, the Benguela Current propagates northwest. Knowing the different sources, the trajectories can be distinguished by the different location of their entry points. In addition to the coloring, we draw the lines segments depending on the distance to the uw-time with decreasing opacity values (Figure 2). The detected upwelling is located mostly in coastal regions, which is a good indication that our filter works well (cf. [MEJ*14]).

4.2. Local Pathline Density

A line-based visualization of a very large number of trajectories can overload the hardware and be too overcrowded to be useful. For a better visualization and better interactive performance, we derived and visualized the local pathline density (**LPD**), which is a scalar field describing the upwelling-relevant flow rate. As before, this visualization analyzes trajectories with the same uw-time. To determine the flow rate, the algorithm performs a cell tracking for every trajectory. For each cell, all intersections of trajectory segments with the cell surfaces are calculated, the lengths of the line segments are derived, summed up and normalized with the cell size.

For the visualization, we first split the trajectories into a part before and after the uw-time. Accordingly, we derived two LPD scalar fields, which we visualized using different colors. The visualization in figure 3 shows a ray casting-based volume rendering of LPD.

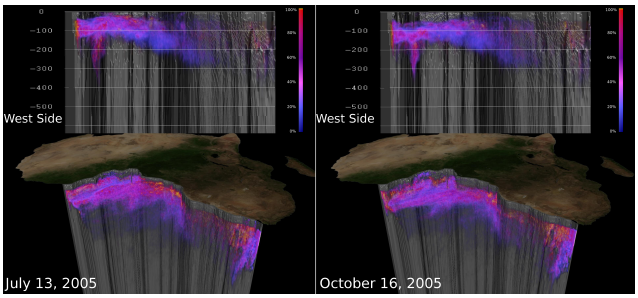

Figure 4: *Visualization of UPR before upwelling for two seasons. Regions with large contributions to ongoing or future upwelling are shaded red/yellow.* ***Top row:*** *side view from the west.* ***Bottom row:*** *3D view.* ***Left****: Shallow UPR (July 13, 2005);* ***Right****: UPR showing upwelling source regions at larger depths (October 16, 2005).*

4.3. Upwelling Particle Ratio

Another approach for trajectory-based upwelling visualization is based on the *upwelling particle ratio* (**UPR**). Contrary to the LPD visualization, visualization of UPR shows the situation at a point in time and not for a time frame. First, for each time step, the current cell index is evaluated for all particles. Using the data of the upwelling trajectories detected before, the algorithm gathers all particles into three groups: 1.) those which currently well up or will well up in future, 2.) those which were welled up, and 3) those which are not welled up at all. The particles belonging to group 1

and 2 are *upwelling particles*. Based on the total number of particles per cell and the number of upwelling particles, we calculated UPR, the ratio between upwelling water and non-upwelling water, for each cell. A separate visualization of UPR for group 1 (before upwelling) and group 2 (after upwelling) allows differentiating between source regions and the further fate of upwelled water. Figure 4 depicts, for two seasons, the spatial structure of UPR for particles before upwelling using volume rendering.

5. Results

For further temporal analysis, we calculated the number of upwelling trajectories for each uw-time. We interpret this value as a measure of upwelling activity, since a large LPD is proportional to transported water mass relevant to upwelling. While the austral winter (June - August) shows strong upwelling activity, minimal activity is found in the austral summer (January - March). Accordingly, the LPD volume rendering shown in figure 3 depicts minimal upwelling for the austral summer and strong upwelling during the austral winter. Besides the density of pathlines representing the flow, the source depth of the water transported is also of interest for upwelling analysis, since it influences water properties such as water temperature, nutrient content or oxygen content.

For a seasonal analysis, the resulting time-dependent data was split into years and visualized as a whisker boxplot, which gives a good impression of the statistically robust seasonal cycle of upwelling activity (Figure 5). At each uw-time of a pathline, an average value for the entering depth and an average value for the maximum depth is stored. Furthermore, we differentiate whether the lines originate at the western or the southern boundary. To visualize the seasonal variations, the two files with the depths stored were split into different years, overlaid and plotted in the form of two whisker boxplots. Figure 6 shows a plot for trajectories originating at the western boundary. First, it is striking that, after entering the domain, the upwelling trajectories increase in depth. Furthermore, there is a increase in depth during the austral winter months, which is later reduced with higher variance between the years. As the additionally submitted video shows, these observations can be reproduced UPR visualizations for the respective seasons.Similar observations could not be made for pathlines originating at the southern boundary as these trajectories encounter upwelling immediately after entering the domain.

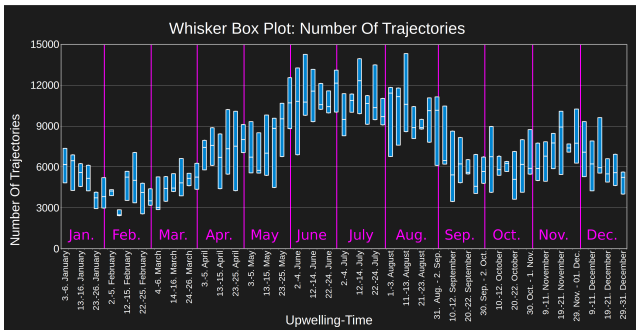

Figure 5: *Whisker boxplot showing the number of upwelling trajectories for each uw-time for the years 2002-2010.*

6. Discussion and Conclusion

Computing the *local pathline density* LPD and the *upwelling particle ratio* UPR facilitates the visual analysis of the spatio-temporal structure of coastal upwelling solely on the basis of the flow field. A temporal analysis of the trajectories selected on the basis of upwelling predicates indicates large seasonal changes in depth and activity of the Benguela upwelling system. The seasonal variability pattern found shows a good correlation with the observed extent of intense Benguela upwelling (cf. figure 4 in [HFAO01]).

However, we also identified potential problems of our approach. The model simulation of Benguela upwelling was carried out using 20 minute time steps, while the data was only stored as 5 day means. These coarser time steps can potentially create an error within the computation of particle pathlines.To evaluate the quality of our pathline integration, we used a synthetic tracer field, which was calculated as part of the model simulation. A tracer can be compared to dye poured constantly at a fixed point and being advected by the flow. This tracer is an unsteady scalar field representing tracer concentration. For evaluation, we selected tracer trajectories running through the source cells of the tracer and calculated the UPR value. A comparison of the original tracer data with our UPR "tracer" data showed a variance of 15% and standard deviation of 4%. These variations could be caused by the methods used or might be the result of the coarse storage interval of the data.

As future work we intend to used advanced integration methods and a further increase in the minimum number of particles per cell. The increased number of particles are straightforward but also more compute-intensive, however, should provide more precise UPR values. Including additional scalar fields such as temperature and biogeochemical quantities to the upwelling detection might further improve the reliability of our method.

Acknowledgements

This work was funded by the German Federal Ministry of Education and Research within the project *Competence Center for Scalable Data Services and Solutions* (ScaDS) Dresden/Leipzig (BMBF 01IS14014B).

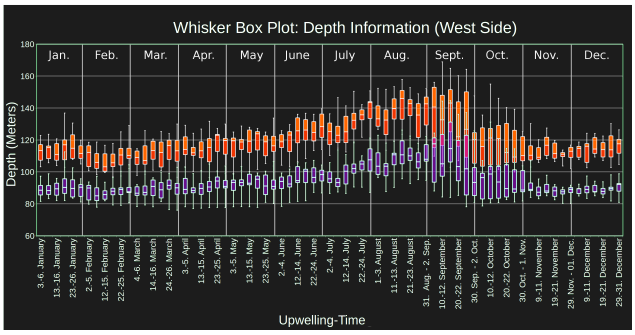

Figure 6: *Whisker boxplot showing the depth of upwelling trajectories for each uw-time for the years 2002-2010. The orange whisker boxes denote the average depth of uw-trajectories entering the domain, the purple ones show the maximum depth of the uw-trajectories before upwelling.*

References

[BMGS13] BORN S., MARKL M., GUTBERLET M., SCHEUERMANN G.: Illustrative visualization of cardiac and aortic blood flow from 4D MRI data. In *2013 IEEE Pacific Visualization Symposium (PacificVis)* (Feb 2013), pp. 129–136. doi:10.1109/PacificVis.2013.6596137. 2

[BPMS12] BORN S., PFEIFLE M., MARKL M., SCHEUERMANN G.: Visual 4d mri blood flow analysis with line predicates. In *2012 IEEE Pacific Visualization Symposium* (Feb 2012), pp. 105–112. doi:10.1109/PacificVis.2012.6183580. 2

[CLSW14] CHAUDHURI A., LEE T. Y., SHEN H. W., WENGER R.: Exploring flow fields using space-filling analysis of streamlines. *IEEE Transactions on Visualization and Computer Graphics 20*, 10 (Oct 2014), 1392–1404. doi:10.1109/TVCG.2014.2312009. 2

[GGD*05] GRIFFIES S. M., GNANADESIKAN A., DIXON K. W., DUNNE J. P., GERDES R., HARRISON M. J., ROSATI A., RUSSELL J. L., SAMUELS B. L., SPELMAN M. J., WINTON M., ZHANG R.: Formulation of an ocean model for global climate simulations. *Ocean Science 1*, 1 (2005), 45–79. http://http://www.ocean-sci.net/1/45/2005/. doi:10.5194/os-1-45-2005. 2

[HFAO01] HAGEN E., FEISTEL R., AGENBAG J. J., OHDE T.: Seasonal and interannual changes in intense benguela upwelling (1982-1999). *Oceanologica Acta 24*, 6 (2001), 557–568. http://www.sciencedirect.com/science/article/pii/S0399178401011732. doi:10.1016/S0399-1784(01)01173-2. 1, 4

[HLH*16] HEINE C., LEITTE H., HLAWITSCHKA M., IURICICH F., DE FLORIANI L., SCHEUERMANN G., HAGEN H., GARTH C.: A survey of topology-based methods in visualization. *Computer Graphics Forum 35*, 3 (2016), 643–667. 2

[Hov49] HOVMÖLLER E.: The trough-and-ridge diagram. *Tellus 1*, 2 (1949), 62–66. http://dx.doi.org/10.1111/j.2153-3490.1949.tb01260.x. doi:10.1111/j.2153-3490.1949.tb01260.x. 2

[HS90] HIBBARD B., SANTEK D.: The VIS-5D system for easy interactive visualization. In *Proceedings of the First IEEE Conference on Visualization: Visualization '90* (Oct 1990), pp. 28–35, 462. http://dl.acm.org/citation.cfm?id=949531.949535. 2

[HSGL11] HERZFELD M., SCHMIDT M., GRIFFIES S., LIANG Z.: Realistic test cases for limited area ocean modelling. *Ocean Modelling 37*, 1-2 (2011), 1–34. http://www.sciencedirect.com/science/article/pii/S1463500311000059". doi:http://dx.doi.org/10.1016/j.ocemod.2010.12.008. 2

[JSM15] JUNKER T., SCHMIDT M., MOHRHOLZ V.: The relation of wind stress curl and meridional transport in the benguela upwelling system. *Journal of Marine Systems 143* (2015), 1 – 6. http://www.sciencedirect.com/science/article/pii/S0924796314002425. doi:10.1016/j.jmarsys.2014.10.006. 3

[KFW16] KANZLER M., FERSTL F., WESTERMANN R.: Line density control in screen-space via balanced line hierarchies. *Computers & Graphics 61* (2016), 29 – 39. http://www.sciencedirect.com/science/article/pii/S0097849316300899. doi:10.1016/j.cag.2016.08.001. 2

[LHD*04] LARAMEE R. S., HAUSER H., DOLEISCH H., VROLIJK B., POST F. H., WEISKOPF D.: The State of the Art in Flow Visualization: Dense and Texture-Based Techniques. *Computer Graphics Forum* (2004). doi:10.1111/j.1467-8659.2004.00753.x. 2

[LHZP07] LARAMEE R. S., HAUSER H., ZHAO L., POST F. H.: *Topology-Based Flow Visualization, The State of the Art*. Springer Berlin Heidelberg, Berlin, Heidelberg, 2007, pp. 1–19. http://dx.doi.org/10.1007/978-3-540-70823-0_1. doi:10.1007/978-3-540-70823-0_1. 2

[MEJ*14] MOHRHOLZ V., EGGERT A., JUNKER T., NAUSCH G., OHDE T., SCHMIDT M.: Cross shelf hydrographic and hydrochemical conditions and their short term variability at the northern benguela during a normal upwelling season. *Journal of Marine Systems 140, Part B* (2014), 92 – 110. Upwelling Ecosystem Succession http://www.sciencedirect.com/science/article/pii/S0924796314001055. doi:10.1016/j.jmarsys.2014.04.019. 1, 2, 3

[MLP*09] MCLOUGHLIN T., LARAMEE R. S., PEIKERT R., POST F. H., CHEN M.: Over Two Decades of Integration-Based, Geometric Flow Visualization. In *Eurographics 2009 - State of the Art Reports* (2009), Pauly M., Greiner G., (Eds.), The Eurographics Association. doi:10.2312/egst.20091062. 2

[MRS*14] MULLER A., REASON C., SCHMIDT M., MOHRHOLZ V., EGGERT A.: Computing transport budgets along the shelf and across the shelf edge in the northern benguela during summer (DJF) and winter (JJA). *Journal of Marine Systems 140, Part B* (2014), 82 – 91. Upwelling Ecosystem Succession. doi:10.1016/j.jmarsys.2014.02.007. 2

[PVH*03] POST F. H., VROLIJK B., HAUSER H., LARAMEE R. S., DOLEISCH H.: The state of the art in flow visualisation: feature extraction and tracking. *Computer Graphics Forum 22*, 4 (2003). 0167-7055. 2

[SE16] SCHMIDT M., EGGERT A.: Oxygen cycling in the northern benguela upwelling system: Modelling oxygen sources and sinks. *Progress in Oceanography 149* (2016), 145 – 173. http://www.sciencedirect.com/science/article/pii/S0079661116301975". doi:http://dx.doi.org/10.1016/j.pocean.2016.09.004. 2

[SGSM08] SALZBRUNN T., GARTH C., SCHEUERMANN G., MEYER J.: Pathline predicates and unsteady flow structures. *The Visual Computer 24*, 12 (2008), 1039–1051. 2

[SS99] SU Y., SHENG Y.: Visualizing upwelling at monterey bay in an integrated environment of gis and scientific visualization. *Marine Geodesy 22*, 2 (1999), 93–103. http://dx.doi.org/10.1080/014904199273515. arXiv:http://dx.doi.org/10.1080/014904199273515, doi:10.1080/014904199273515. 2

[SS06] SALZBRUNN T., SCHEUERMANN G.: Streamline predicates. *IEEE Transactions on Visualization and Computer Graphics 12*, 6 (2006), 1601–1612. 2

[SW15] SPRENGER M., WERNLI H.: The LAGRANTO lagrangian analysis tool – version 2.0. *Geoscientific Model Development 8*, 8 (2015), 2569–2586. http://www.geosci-model-dev.net/8/2569/2015/. doi:10.5194/gmd-8-2569-2015. 2

[SWJS08] SALZBRUNN T., WISCHGOLL T., JAENICKE H., SCHEUERMANN G.: The state of the art in flow visualization: Partition-based techniques. In *Simulation and Visualization* (2008), pp. 75–92. 2

[TZH15] TIM N., ZORITA E., HÜNICKE B.: Decadal variability and trends of the benguela upwelling system as simulated in a high-resolution ocean simulation. *Ocean Science 11*, 3 (2015), 483–502. URL: http://www.ocean-sci.net/11/483/2015/, doi:10.5194/os-11-483-2015. 1, 2